Morphology and Organization of Poly(propylene imine) Dendrimers in the Melt from Molecular Dynamics Simulation

Nikolas Zacharopoulos and Ioannis G. Economou*

Molecular Modelling of Materials Laboratory, Institute of Physical Chemistry, National Research Centre for Physical Sciences "Demokritos", GR-15310 Aghia Paraskevi Attikis, Greece

Received June 1, 2001; Revised Manuscript Received November 1, 2001

ABSTRACT: Molecular dynamics simulations are performed on generations 2 (*G*2) through 5 (*G*5) of poly(propylene imine) dendrimers at 400 K in order to investigate characteristics of molecular structure and morphology in the melt. As the generation increases, the dendrimers assume a more spherical shape, and the degree of dendron overlap increases, albeit at a decaying rate. The distribution of end groups within the molecule widens with *G* and separates at *G*5 into inner (back-folded), intermediate, and outer rims. Back-folded branches are accommodated by the increased extension of the initial spacers. Furthermore, the radius of gyration scales approximately with the cubic root of the number of monomers. Finally, interpenetration of individual dendrimer molecules decreases with generation. Simulation results are in good agreement with the limited experimental data available.

Introduction

Dendrimers are highly ordered, well-defined branched polymers, with segments between branch points (spacers) comprising relatively short chains. Their treelike structure is formed by a stepwise, iterative reaction sequence of the functional groups in each generation starting from and radiating out from a smaller, multifunctional initiator core molecule from which the main branches or dendra emanate.[1,2] When the recursive process leads to complete shells for each generation, monodisperse polymers are fabricated that have a defined number of end groups, and their size and architecture are specifically controlled in the synthesis. Dendrimers find potential use in nanoscale catalysis, as micelle mimics, supramolecular building blocks, molecule encapsulation and delivery agents, etc.[3] A key aspect in all these applications is the understanding of the molecular structure, particularly the end group distribution within the dendrimer molecule, information needed to guide the design and synthesis.

The location of the terminal groups has been a point of controversy in the literature starting with the study of de Gennes and Hervet[4] who made the assumption of fully extended branches with the end groups on the periphery of the molecule predicting a limiting generation due to steric hindrance. The congestion at the surface is due to the fact that the number of end groups grows exponentially with generation while the surface of the molecule increases as the radius (proportional to the generation in the fully extended model) squared. The picture of the end groups lying on the periphery is supported by X-ray scattering experiments;[5] however, studies based solely on radius of gyration data have been shown to be inconclusive.[6] In addition, resonance techniques are limited in their ability to resolve the resonances from the many unique but very similar groups in the molecule. So far, conventional 1-d NMR data[7,8] have provided evidence of proximity of the terminal groups to the dendrimer core. Recently, a 3-d NMR technique was used to separate the overlapping H resonances from the core, interior and exterior methylene groups of third generation poly(propelene imine) (PPI) dendrimers,[9a] thereby allowing for experimental data on the arrangement of dendra without the need to resort to isotopic labeling. Using this technique, it was shown that PPI dendrimers assume different conformations in polar and nonpolar solvents.[9b] Simulations and theoretical models applied to dendrimer solutions, for the most part, produce an even distribution of end groups throughout the molecule and a density profile that decreases outward from the core.[10−15]

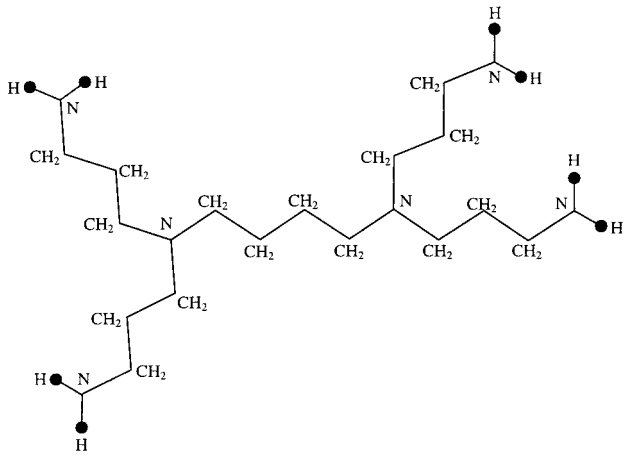

Figure 1. Schematic representation of the model PPI *G*1 dendrimer. The methylene groups are treated as united atoms.

In the present study, we investigate the structural features of a widely studied and commercially available dendrimer, namely PPI formed of a binary core of 1,4-diaminobutane, to obtain detailed information on the size and internal organization of the molecule. To this end, we employ molecular dynamics (MD) simulations of the dendrimer in the molten state, using an atomistic force field to account for the interactions. To our knowledge, this is the first published work on atomistic simulation of dendrimer melts. Melt properties will be used as reference in future studies of solution properties for the same dendrimer in different solvents.

* Corresponding author. E-mail: economou@mistras.chem.demokritos.gr. Telephone: ++ 30 1 6503963. Fax: ++ 30 1 6511766.

10.1021/ma010953x CCC: $22.00
Published on Web 02/01/2002

Table 1. Parameters of the DREIDING Force Field[16] for the Atoms Examined in This Work

	bond stretching[a]		bond bending[b]		Lennard-Jones[c]	
atom type i	b_i^0 (Å)	k_{b_i}(kcal/mol/Å^2)	θ_i^0 (deg)	k_{θ_i}(kcal/mol/rad^2)	σ_i (Å)	ϵ_i (kcal/mol)
H	0.330	700	180.0	$100/(\sin\theta_i^0)^2$	3.1950	0.0152
N	0.702	700	106.7	$100/(\sin\theta_i^0)^2$	3.6621	0.0774
CH_2	0.770	700	109.471	$100/(\sin\theta_i^0)^2$	4.0677	0.1984

[a] $b_{ij}^0 = b_i^0 + b_j^0 - \delta$; $\delta = 0.01$ Å. [b] For $\theta_i^0 = 180°$, the bending term in eq 1 is $k_{\theta_i}(1 + \cos\theta_i)$; $k_{\theta_i} = 100$ kcal/mol/rad^2. [c] $\epsilon_{ij} = (\epsilon_i\epsilon_j)^{1/2}$; $\sigma_{ij} = (\sigma_i + \sigma_j)/2$. Torsion: sp^3-sp^3: $k_{\phi_i} = 2.0$ kcal/mol, $n_i = 3$, $\varphi_i^0 = 180^0$. sp^3-sp^2: $k_{\phi_i} = 1.0$ kcal/mol, $n_i = 6$, $\varphi_i^0 = 0^0$.

Simulation Details

All simulations presented in this work were performed using the Cerius[2] software package of Accelrys Inc. (previously known as Molecular Simulations Inc.). Figure 1 shows a schematic representation of the molecular model for a first generation PPI dendrimer. The DREIDING force field[16] was used to describe the intra- and intermolecular interactions. It has the following general form:

$$E = \frac{1}{2}\sum_{i}^{\text{all bonds}} k_{b_i}(b_i - b_i^0)^2 + \frac{1}{2}\sum_{i}^{\text{all bond angles}} k_{\theta_i}(\cos\theta_i - \cos\theta_i^0)^2 + \frac{1}{2}\sum_{i}^{\text{all torsional angles}} k_{\phi_i}\{1 - \cos[n_i(\phi_i - \phi_i^0)]\} + \sum_{i,j}^{\text{all non-bonded sites}} \epsilon_{ij}\left[\left(\frac{\sigma_{ij}}{r_{ij}}\right)^{12} - 2\left(\frac{\sigma_{ij}}{r_{ij}}\right)^{6}\right] \quad (1)$$

The first three terms in the sum account for bond stretching, bond bending, and dihedral angle rotation around the equilibrium values b^0, θ^0, and ϕ^0, respectively. The last term accounts for the nonbonded dispersion interactions expressed by the Lennard-Jones potential; a cutoff distance of 1.0 nm is used, with a cut-in distance for a spline switching method set to 0.9 nm. The constants and geometric parameters in DREIDING are defined with consideration to the hybridization of the atom types rather than the specific combination of atoms. In this work, methylene groups are treated as united atoms. This approach reduces the computational time significantly without reducing the accuracy of the calculations. The constants and parameters for the relevant atom types are presented in Table 1. Periodic boundary conditions were used to simulate the melt, with the system size kept at around 2500 interaction sites. In this way, melts of 36, 17, 8, and 4 molecules were examined for generations 2, 3, 4, and 5, respectively. The initial system density was chosen to be 1.06 g/cm^3, yielding a simulation cell edge of about 25 Å.

In all cases, the energy was initially minimized using a hundred steps of steepest descent followed by 4000−5000 steps of conjugate gradient to relax the structure. The melt was then subjected to MD simulated annealing of five repeat cycles from 400 to 700 K and back, in steps of 50 K, spending 2 ps in each step under *NPT* conditions (with pressure equal to 1 atm) to release the molecules from potential configurational traps or initial biases. The energy was minimized at the end of each annealing cycle via molecular mechanics. The ensuing *NPT* MD simulation consisted of a 100 ps long equilibration run, followed by a data collection run of 400 ps at 400 K and 1 atm. The integration time step was chosen to be 1 fs while trajectory data were stored every 100 time steps. The simulations proceeded at a rate of approximately 14 min of CPU time for each simulated ps on a SGI Indigo2 R10000 processor at 195 MHz.

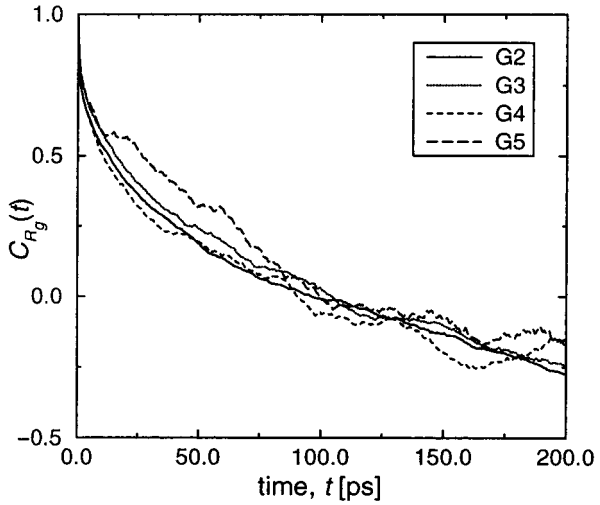

Figure 2. Autocorrelation function of the squared radius of gyration.

Results and Discussion

The relaxation process described above resulted in stabilizing the energy and the radius of gyration, R_g, of the dendrimer, averaged over all molecules. Equilibrium values were reached within the first 50 ps. To examine the relaxation of dendrimer molecules, the autocorrelation function of the squared radius of gyration, $C_{R_g}(t)$, was evaluated from the expression:

$$C_{R_g}(t) = \frac{\langle (R_g^2(t) - \langle R_g^2\rangle)(R_g^2(0) - \langle R_g^2\rangle)\rangle}{\langle R_g^4\rangle - \langle R_g^2\rangle^2} \quad (2)$$

Results are shown in Figure 2 for the four generations considered. From these data, a relaxation time, t_{R_g}, where $C_{R_g}(t_{R_g}) = 1/e$, is calculated. The t_{R_g}values calculated were 24 ps for *G*2, 29 ps for *G*3, 20 ps for *G*4 and 45 ps for *G*5 dendrimer. With the exception of *G*4, we observe that, the relaxation time increases with the generation, in accordance also with previous simulation studies.[11] *G*4 represents the threshold generation of extended growth of the branches, with enough space available for large-scale maneuvering and subsequent resizing, as will be further elaborated later on.

MD simulations by Murat and Grest[11] for dendrimer solutions where the solvent was of varying quality resulted in relaxation times for *G*5 dendrimers in the range 25−70 τ, going from poor to athermal solvent, where $\tau = \sigma(m/\epsilon)^{1/2}$ is the natural time unit. Substitution of the average values for σ, m, ϵ for the atom types in the model considered here yields a relaxation time of 45−125 ps. Although quantitative comparison is not

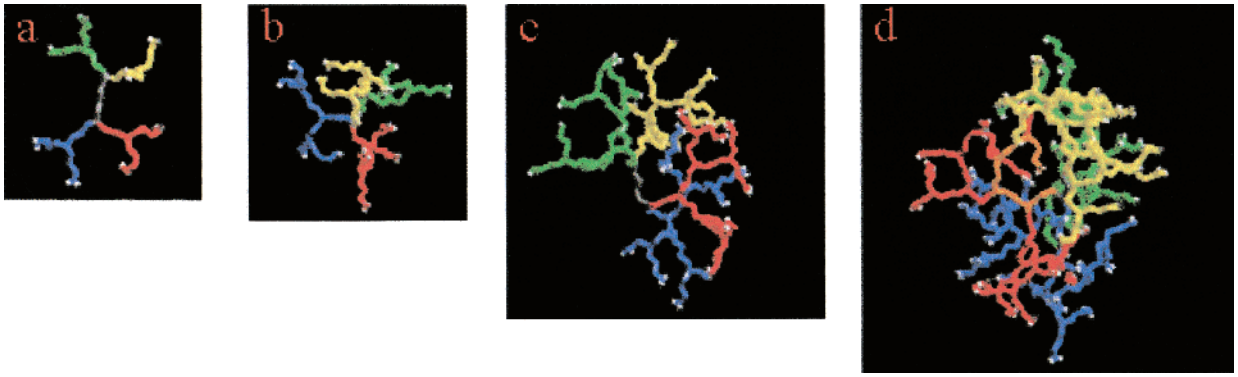

Figure 3. Typical equilibrated (t = 500 ps) conformations of generations $G2$ through $G5$. The colors represent the four dendra emanating from the gray core. The terminal hydrogens are depicted white.

possible because the molecular model used by Murat and Grest is different than the model used here, the agreement between the two sets of simulation is considered acceptable.

For all the systems examined here, the production run was divided into blocks of 80 ps. In the figures that follow, the data points represent the average and the error bars the standard deviation of the five blocks. The values reported here correspond to averages over all dendrimers included in the melt of the respective generation.

Typical equilibrated conformations of the four dendrimer generations examined here are shown in Figure 3. The different colors represent the four dendra stemming from the two ends (roots) of the dendritic core (gray), whereas the hydrogens of the end-groups are depicted white. As the generation number increases the molecule becomes more compact, and the dendra, subdendra, etc. turn inward, exhibiting a behavior fundamentally different from that observed for the lower generations characterized by extended branches. In addition, beyond the second generation there is a departure from the nearly two-dimensional shape, progressing from a tetrahedral (at the third generation) toward a more spherical spatial organization at the higher generations. The change in shape is reflected on the relative shape anisotropy, κ^2, defined as[17]

$$\kappa^2 = 1 - \frac{3I_2}{I_1^2} \tag{3}$$

where I_1 and I_2 are the first and second invariants of the radius of gyration tensor. This quantity assumes values between 1 (for a linear array of atoms) and 0 (for shapes of high 3-d symmetry). As shown in Figure 4, this quantity equals approximately 0.22 ($\kappa^2 = {}^1/_4$ for planar arrays) for second generation dendrimers and progressively decreases for higher generations (except for a small rise at $G4$, within the statistical uncertainty).

The overall dendrimer shape is inherently linked to the arrangement of the dendra within the molecule. To elucidate the internal structure of the dendrimers, we first analyzed their local conformation by examination of the dendron expansion pattern. More specifically, we measured the relative expansion, S, of sequential spacers by taking the projection of spacer vector $\boldsymbol{I}_{m+1}$ on spacer vector $\boldsymbol{I}_m$ (as defined graphically in the inset of Figure 5), where m and $m + 1$ are sequential branch points, normalized by the theoretical spacer length, l,

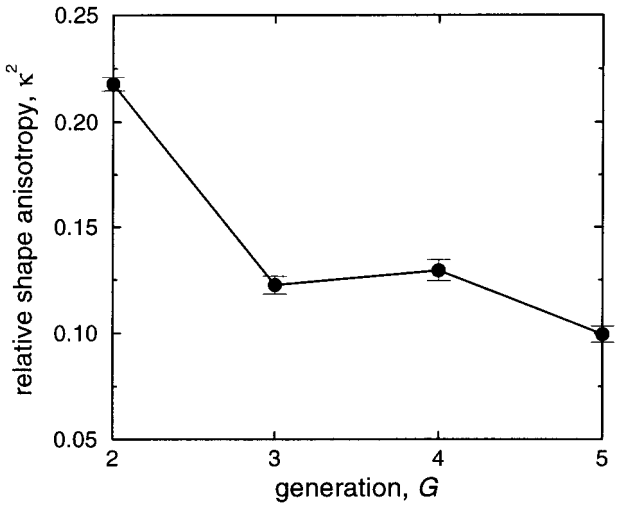

Figure 4. Relative shape anisotropy (see text) as a function of dendrimer generation.

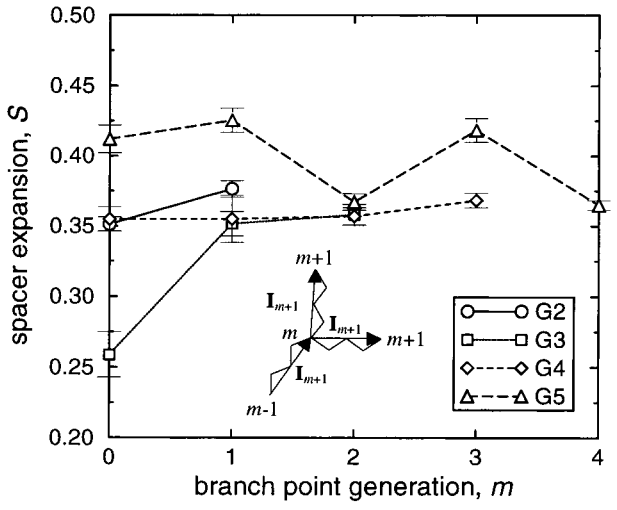

Figure 5. Spacer expansion, S, defined as the projection of vector $\boldsymbol{I}_{m+1}$ on vector $\boldsymbol{I}_m$, normalized by the all-trans spacer length, as function of branch point generation, m, for $G2$ through $G5$.

in an all-trans conformation (0.489 nm in this case):

$$S = \frac{\boldsymbol{I}_{m+1} \cdot \boldsymbol{I}_m}{|\boldsymbol{I}_m| l} \tag{4}$$

The spacer expansion, incorporating the effects of bond and torsional angles and of bond length on spacer

expansion, is plotted against the index of the common branch point, identifying the generation number m within the dendrimer, or the topological distance (in spacers) of the branch point from the respective root. Vector $\boldsymbol{I}_0$ is the end-to-end vector of the initiator core molecule, and its direction is taken such that it is always in a head-to-tail connection with the respective $\boldsymbol{I}_1$. A similar analysis has been performed in the theoretical study of Ganazzoli et al.[15] for dendrimer solutions based on a more coarse-grained model than the one here, that is freely jointed chains. The local conformation in their case was expressed as the scalar product of sequential bond vectors of unit length in a head-to-tail connection ($\langle \boldsymbol{I}_m \cdot \boldsymbol{I}_{m+1} \rangle$). In this theoretical treatment, a parabolic expansion was found for the case of a one-bond long spacer, with a maximum at $m = 1$ or $m = 2$ displaced to larger values along the ordinate with generation number G due to increased crowding of the end groups. This regular picture of expansion is largely owed to the stiff bonds connecting consecutive branch points and, as an average trend, persists even in the case of the slightly less rigid two-bond-long spacer.

The results of Figure 5 show the departure from regularity due to the highly flexible four-bond spacers. In all but the highest generation G, the expansion shows a relative increase as we move up the dendron in generation m, as spacers are forced to expand in a more confined environment. This is in agreement with the general concept of de Gennes and Hervet in which the spacers closer to the core are less extended than the ones near the periphery[4] (however, in our case, the proximity is topological not spatial). Moreover, the values for the three lower generations G are very close (hinting to similar internal structure). The only anomaly observed is in the low expansion of the first spacer of $G3$. Steric congestion on the plane forces the third generation to expand into the third dimension which for this generation is considerably open. The dendrimer assumes a structure that resembles a tetrahedron by torsion of the bonds in the first spacer. This shape, observed elsewhere in the literature,[18,19] brings apart most efficiently branch points of higher m. In generation $G4$, the tetrahedral organization leads to crowding, and higher symmetry structures are formed, characterized by an even distribution of spacer expansion along the dendron. Extended spread of dendra is no longer sustainable in $G5$ dendrimers, thus producing a back-folding which is manifested as bending at the branch points of $m = 2$ and $m = 4$. This behavior is readily visible in the conformation of $G5$ of Figure 3 by tracing the succession of spacers leading from the core to the terminal group depicted orange. The initial spacer assumes a more extended conformation than at lower G, thereby forming an inner cavity where the back-folded branches are accommodated.

The spatial arrangement of branch points as a function of their topological distance from the respective root is presented in Figure 6. For the lower dendrimer generations the rate at which the branch points expand from the center of mass as a function of branch point generation, m, shows an increase up to $m = 2$ and then starts to drop. In the case of $G5$ dendrimers this rate is a monotonically decreasing function of the topological distance. Furthermore, comparison of the curves of $G2$ and $G5$ alludes to similar extended growth of initial spacers relative to the more confined expansion of $G3$ and $G4$. This extended organization in the case of $G2$ is

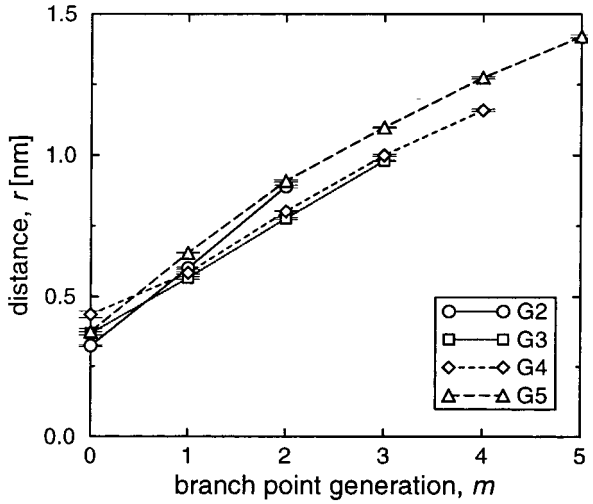

Figure 6. Branch point distance from the center of mass as a function of topological distance from the core for generations $G2$ through $G5$.

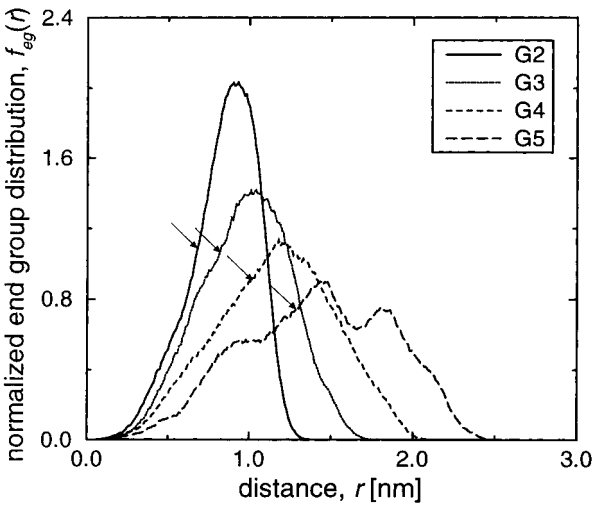

Figure 7. Normalized distribution of end groups as a function of distance from the center of mass for $G2$ through $G5$. The arrows point to the position of the radius of gyration of the respective dendrimer generation.

due to the absence of crowding, whereas in the case of $G5$ it arises out of necessity for creating adequate available space to host the back-folded branches.

Further information on the arrangement of dendra within the dendrimer molecule can be obtained from the distribution of end groups, normalized by the number of end groups in each generation, as a function of core distance, presented in Figure 7. Going from the lowest to the highest generation, the end groups spread more uniformly over a widening range centered at an ever-decreasing distance from the radius of gyration of the dendrimer (marked with arrows). Moreover, the transition from extended to inward bent branches is evidenced by the change in distribution from unimodal at lower G to trimodal at $G5$. The bulk of the end groups is still inhabiting a shell in the vicinity of R_g, but there is considerable increase in their numbers at the periphery and in the inner regions of the dendrimer. Although dendrimers with $G > 5$ were not investigated in the present study, we expect that, for higher generations the region around R_g will become depleted of end groups, giving rise to a bimodal distribution with end groups placed close to the core and on the surface of the

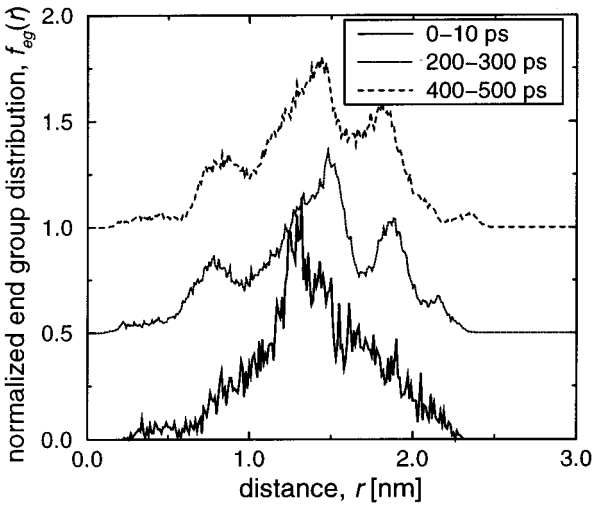

Figure 8. Normalized distribution of end groups for a single *G*5 dendrimer as a function of distance from the center of mass averaged over three separate periods of the simulation run. The curves are relatively displaced along the vertical axis by 0.5 for clarity.

molecule.[20] Figure 8 shows the distribution of end groups for a single *G*5 dendrimer averaged over the first 10, 200−300, and 400−500 ps. The three curves are relatively displaced along the ordinate by 0.5 for clarity. As the structure relaxes, the distribution departs from the energetically unfavorable high concentration around R_g, and the dendra self-organize into the trimodal state.

The radial number density distribution of the entire dendrimer molecule is depicted in Figure 9a. The density is calculated by drawing concentric spheres around the center of mass, incrementing the radius by 0.01 nm, and counting the number of segments within a spherical shell. The curve corresponding to *G*2 exhibits a monotonic decrease, briefly interrupted by a shoulder around the position of the $m = 0$ branch point (cf. Figure 6). The shoulder is revealing of the branched architecture and of the extended conformation of the dendra at *G*2. The density for the higher generation dendrimers is characterized by a drop at distances very close to the center of mass, followed by a sharp rise. This behavior is due to the higher degree of space filling beyond *G*2. The transition from the lower to the higher density values narrows and sharpens substantially at *G*5 as a consequence of back-folding. In addition, there is a region of small slope density drop, spread over the range of the first mode in the distribution of end groups (compare to Figure 7). The contribution of the final *m* generation to the overall density is readily captured in Figure 9b which shows the end group number density distribution. Finally, we note in Figure 9a that all *G*s seem to pass through the same density at around 0.167 nm, a value close to the theoretical bond length (0.153 nm).

The results for the complete density profile are in qualitative agreement with mean field models,[21] lattice[12,13] and hard sphere[22] Monte Carlo simulations, and coarse[11] and atomistic[8,20,23] MD simulations. All these studies predict that dendrimer density decays outward from the center of mass with terminal groups distributed all throughout the molecule. However, only the MD studies reported evidence of multimodal distribution of end groups. In most of the literature data above, the entire segment density of the terminal *m* generation was computed, rather than the isolated end group density

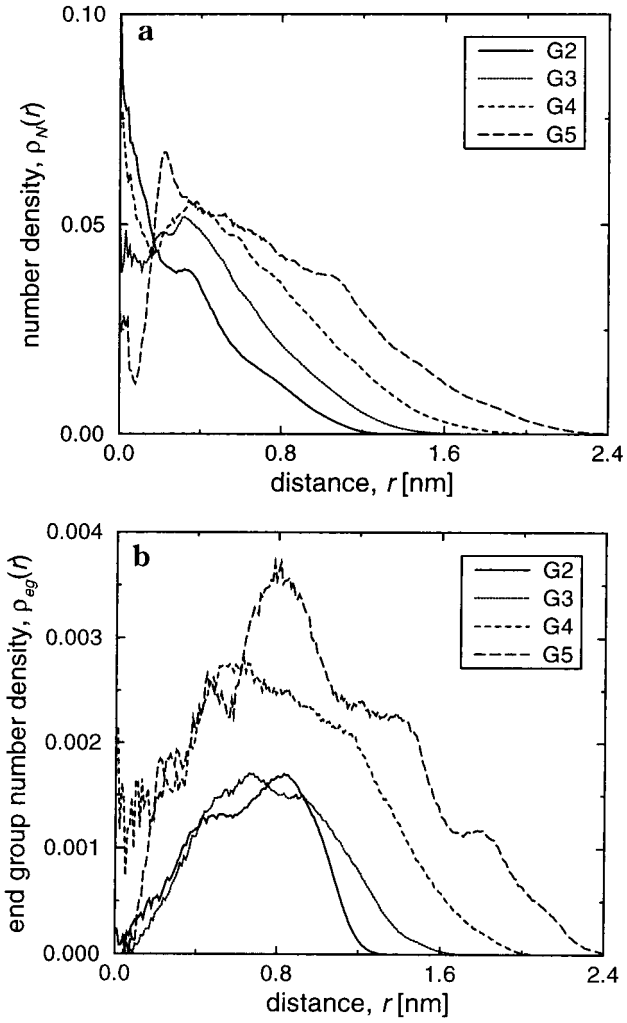

Figure 9. Radial number density distribution of (a) the entire molecule and (b) the end groups for generations *G*2 through *G*5.

reported here. Therefore, inherent peaks in the density might have spread out over a wider range of distances accounting for the delocalized nature of an entire terminal spacer.

From the MD results, the amount of overlap of the four dendra within the dendrimer molecule was calculated. The dendrimer volume was divided into cubic cells of edge length 0.4 nm, with the origin placed at the center of mass. The occupancy of the cell identified by the indices *i*, *j*, *k* by an atom belonging to dendron α (α ranging from one to four) is defined as $\psi_\alpha(i,j,k)$, and can take the values 0 (unoccupied) or 1 (occupied). The total overlap, O_t, is determined from

$$O_t = \frac{2}{3}\frac{\sum_{\{i,j,k\}}\sum_{\alpha\neq\beta}\langle\psi_\alpha\psi_\beta\rangle}{\sum_{\{i,j,k\}}\sum_{\alpha=\beta}\langle\psi_\alpha\psi_\beta\rangle} \quad (5)$$

where the averages are over all configurations, and takes values between 0 and 1. This calculation is similar to a procedure introduced by Murat and Grest,[11] the main difference being that, in their work, averaging takes place outside the product. Averaging over the occupancy of a cell by each of the dendra separately and then calculating the product can lead to erroneous

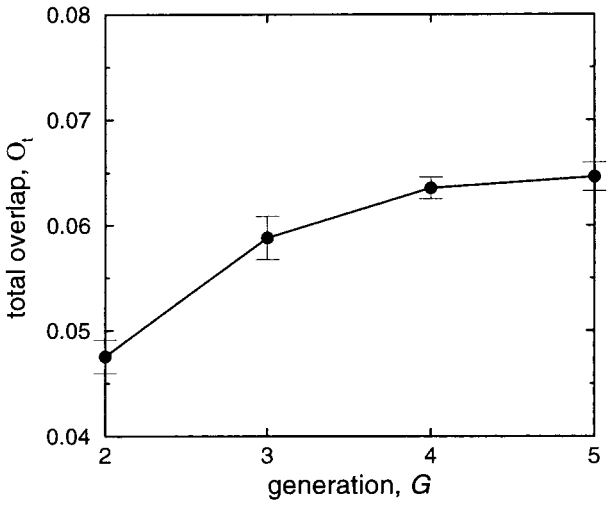

Figure 10. Total dendron overlap as a function of dendrimer generation.

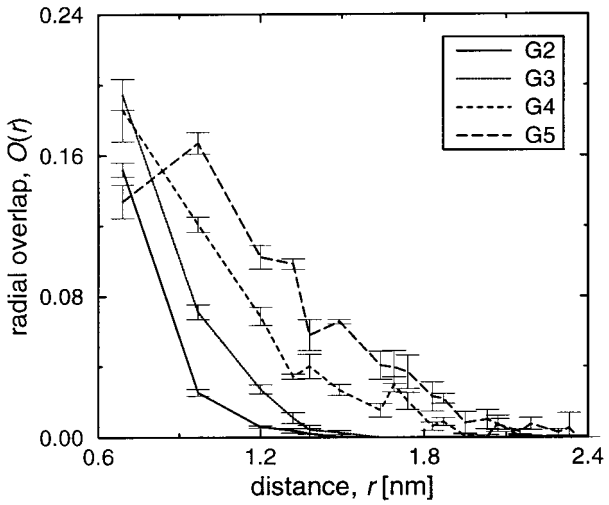

Figure 11. Radial dendron overlap for generations *G*2 through *G*5.

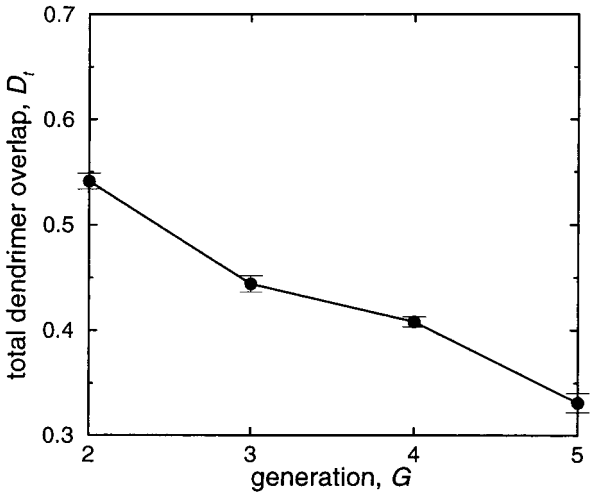

Figure 12. Total dendrimer overlap as a function of dendrimer generation.

results, since overlap is defined as the *simultaneous* occupancy of space: the occupancy events are *not* independent. The quantity described by eq 5 varies between complete overlap, when there is coexistence of all dendra contributing at least one atom each in every occupied cell, to complete segregation, when cell occupancy is owed exclusively to atoms of a single dendron. As shown in Figure 10, the overlap increases with *G*, and apparently reaches a plateau. This behavior is consistent with the picture of the dendrimer molecule assuming a compact spherical shape at higher generations, with the dendra interpenetrating at the surface (*G*4) and/or close to the core because of back-folding (*G*5). The trend followed here is the reverse of that observed by Murat and Grest for the case of dendrimer solutions,[11] mainly due to the difference in the methods used to calculate overlap. As the generation increases, the motion of individual dendra in an ever more confined environment leads to a decreased coverage of overall volume, i.e., to a decreased occupancy by each dendron. However, the number of cells that host segments of different dendra increases in denser surroundings; i.e., actual dendron overlap increases. Along the same lines, the conjecture by Mansfield[24] that dendra should overlap at the limiting generation, is corroborated by our results.

To locate dendron overlap within the molecule, we evaluated the radial overlap $O(r)$ in a manner similar to O_t summing only over the cells that lie at a discrete distance r from the center of mass[11]

$$O(r) = \frac{2}{3}\frac{\sum_{\{i,j,k\}}\sum_{\alpha\neq\beta}\langle\psi_\alpha\psi_\beta\rangle\delta_{r,r_{i,j,k}}}{\sum_{\{i,j,k\}}\sum_{\alpha=\beta}\langle\psi_\alpha\psi_\beta\rangle\delta_{r,r_{i,j,k}}} \qquad (6)$$

This quantity is plotted in Figure 11 for the four generations examined. Moving toward the outside of the molecule the dendra become completely disentangled either monotonically with distance (*G*2, *G*3), or with intermediate kinks at the periphery (*G*4) and/or close to the core (*G*5) corresponding to localized overlap. In particular, the low initial value of *G*5 reflects the extended conformation of the $m = 1$ spacer (cf. Figure 5), while the maximum overlap at this generation occurs around the first mode in the end group distribution where the density is highest (cf. Figures 7 and 9b).

The picture of overlap is completed with an analysis of the interpenetration of the dendrimer molecules. A method similar to the one described above was used, with total dendrimer overlap, D_t, being calculated by summation over all dendrimers of the averages of the product $\psi_A\varphi_A$, where ψ_A is the occupancy of a cell by dendrimer A and φ_A the occupancy of the same cell by *any* dendrimer *other* than A

$$D_t = \frac{\sum_{\{i,j,k\}}\sum_{A}\langle\psi_A\varphi_A\rangle}{\sum_{\{i,j,k\}}\sum_{A}\langle\psi_A\psi_A\rangle} \qquad (7)$$

ψ_A and φ_A are assigned the values 0 or 1 reflecting the absence or presence of dendrimer segments, respectively. The results of this analysis are depicted in Figure 12 as a function of the generation number. The trend followed is the reverse of that demonstrated by dendron overlap, with interpenetration decreasing with increasing generation. This result is expected on the basis of the previous discussion of dendrimer compactness at higher generations. Investigation of the localized den-

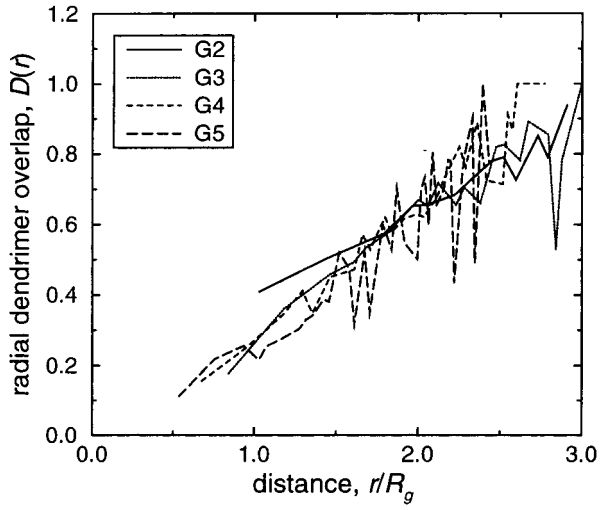

Figure 13. Radial dendrimer overlap for generations *G*2 through *G*5.

drimer overlap as a function of the reduced distance from the center of mass of dendrimer A shown in Figure 13 reveals a very similar behavior for all generations, demonstrating a monotonic increase toward the periphery of the molecule. The higher value for *G*2 at small distances is owed to the considerably more open and nearly flat structure of the particular generation.

The dendrimer melt adapts well to the study of the scaling behavior as it produces conformations resembling the ones that result from the Θ state. Chen and Cui,[25] who conducted Monte Carlo simulations on a model of freely rotating rigid bonds, observed that the scaling regime shrinks with increasing generation. They concluded that the correct scaling exponent for a high *G* dendrimer can, in fact, be obtained by reducing the effects of excluded volume (close to the Θ point). Figure 14a shows the variation in the radius of gyration as a function of generation number compared to SANS data of PPI in 1% v/v in D_2O.[20] Although simulation results are generally in reasonable agreement with experimental data, the deviation from experiment increases with generation number in accord with the MD results by Scherrenberg et al.[20] The simulation data are plotted as a function of segment number, *N*, on a log−log scale in Figure 14b, along with the experimental results. The solid line is the best fit to a power law dependence with an exponent equal to 0.29. This scaling exponent, although higher than what is predicted by theory[4,15] and earlier simulation,[10] is in excellent agreement with the results of Mansfield and Klushin[12] (0.29 for their "augmented" dendrimers) and of Murat and Grest[11] (0.29 for $T = \Theta$). Last, we note that the size of phantom dendrimers may be calculated analytically by means of the Wiener index.[26] This is a topological invariant of a molecular graph of *n* vertexes that is related to the unperturbed radius of gyration by $W(n) = n^2\langle R_g{}^2 l^{-2}\rangle$, where *l* is the bond length. Using the analytical form of the Wiener index for *monocentric* dendrimers[27] together with an average value for the bond length, we estimate a dependence of the radius of gyration, $R_g \propto N^{0.31}$. The scaling exponent is very close to the value of 0.29 for our *dicentric* dendrimer for which the Wiener index differs only by a fairly constant multiplier.[28]

Finally, the fractal dimension of the dendrimer in each generation was calculated from its respective number density profile, $\rho_N(r)$ (Figure 9a), using the

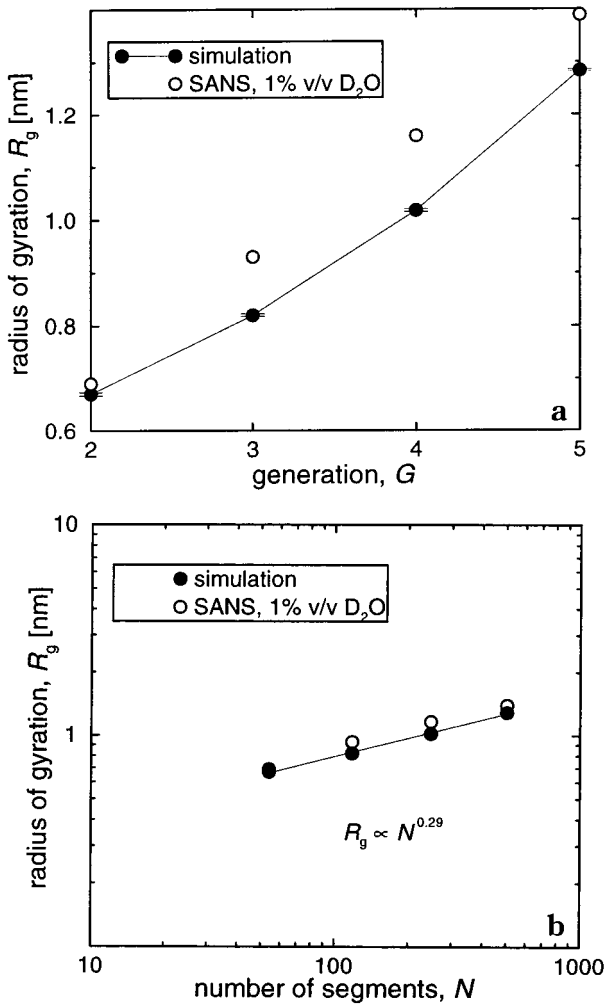

Figure 14. Experimental data[20] and simulation results for the PPI dendrimer radius of gyration as a function of (a) dendrimer generation, and (b) number of segments.

method suggested by Murat and Grest,[11] which relates the radial segment number, $N(r)$, with the distance from the center of mass

$$N(r) = 4\pi\int_0^r r'^2 \rho_N(r')\mathrm{d}r' \qquad (8)$$

The exponent extracted from a log−log plot of $N(r)$ is 2.56, 2.95, 2.88, and 3.09 in order of increasing generation *G*. The relatively increased fractality at *G*3 is consistent with the results of Figure 4: the tetrahedral structure of these dendrimers allows them to fill space more effectively than their *G*4 counterparts. The fractal dimensions are presumably higher than those of Mansfield[13] (generations six through nine were reported) and closer to the ones calculated by Murat and Grest.[11] The value of 3.09 at *G*5 further supports the notion of a compact molecule at higher generations.

Conclusions

We have performed molecular dynamics simulations on dendrimers of generations two through five in the molten state. The properties investigated aim at gaining insight on the internal organization of the dendritic molecule. In particular, the determination of spacer expansion demonstrates that there exists a critical generation (*G*5 in the case of PPI), at (and beyond) which the outward extended dendra of the lower gen-

eration dendrimers grow partially organized in a back-folded arrangement. The end group density distribution, which shows the reinforcement of the regions close to the center of mass and the periphery, completes a picture of dendrimers of higher generations comprising heavily extended and back-folded branches. We speculate that at the limiting generations the bimodal distribution prevails.

The overall density profiles exhibit a gradual decrease from the center of mass toward the surface of the molecule. At the critical generation where back-folding becomes evident, the density shows a sharp well near the core and a smooth decay on the molecular periphery, interrupted by a region of reduced slope. Related to the density is the entanglement of the dendra, which appears to grow with generation, albeit at an ever-decreasing rate, supporting the picture of a compact, space-filling molecule at the higher generations. Due to the higher degree of packing, interpenetration of individual molecules decreases with generation. Further evidence of space-filling is provided from the variation of the fractal dimension with generation reaching the spatial dimension for *G*5. Finally, the molecule approaches a spherical shape as it grows in generation. Dendrimer size is shown to scale with the number of segments as $N^{0.29}$. Current work focuses on the structure and morphology of PPI in solution.

Acknowledgment. We are indebted to Professor Doros Theodorou for invaluable suggestions and discussions regarding this work. We thank Accelrys, Inc. for making their Polymer Consortium software available to the Molecular Modelling of Materials Laboratory through an agreement with Professor Doros Theodorou. Financial support of this work by the PENED-99 program of the Greek Secretariat of Research and Technology (GSRT) is gratefully acknowledged.

References and Notes

(1) Fréchet, J. M.; Hawker, C. J. In *Comprehensive Polymer Science*, 2nd suppl., Aggarwal, S., Russo, S., Eds.; Pergamon Press: Oxford, England, 1996; pp 234−298.
(2) Newkome, G. R.; Moorefield, C. N.; Vögtle, F. *Dendritic Molecules. Concepts, Syntheses, Perspectives*; VCH: Weinheim, Germany, 1996.
(3) Bosman, A. W.; Janssen, H. M.; Meijer, E. W. *Chem. Rev.* **1999**, *99*, 1665−1688.
(4) de Gennes, P.-G.; Hervet, H. J. *J. Phys. Lett. Fr.* **1983**, *44*, L351-L360.
(5) Topp, A.; Bauer, B.; Klimash, J. W.; Spindler, R.; Tomalia, D. A.; Amis, E., J. *Macromolecules* **1999**, *32*, 7226−7231.
(6) Lyulin, A. V.; Davies, G. R.; Adolf, D. B. *Macromolecules* **2000**, *33*, 6899−6900.
(7) Wooley, K. L.; Klug, C. A.; Tasaki, K.; Schaefer, J. *J. Am. Chem. Soc.* **1997**, *119*, 53−58.
(8) Gorman, C. B.; Hager, M. W.; Parkhurst, B. L.; Smith, J. C. *Macromolecules* **1998**, *31*, 815−822.
(9) (a) Chai, M.; Niu, Y.; Youngs, W. J.; Rinaldi, P. *Macromolecules* **2000**, *33*, 5395−5398. (b) Chai, M.; Niu, Y.; Youngs, W. J.; Rinaldi, P. L. *J. Am. Chem. Soc.* **2001**, *123*, 4670−4678.
(10) Lescanec, R.; L., Muthukumar, M. *Macromolecules* **1992**, *25*, 2401.
(11) Murat, M.; Grest, G. S. *Macromolecules* **1996**, *29*, 1278−1285.
(12) Mansfield, M. L.; Klushin, L. I. *Macromolecules* **1993**, *26*, 4262−4268.
(13) Mansfield; M. L. *Macromolecules* **2000**, *33*, 8043−8049.
(14) Boris, D.; Rubinstein, M. *Macromolecules* **1996**, *29*, 7251−7260.
(15) Ganazzoli, F.; La Ferla, R.; Terragni, G. *Macromolecules* **2000**, *33*, 6611−6620.
(16) Mayo, S. L.; Olafson, B. D.; Goddard, W. A., III. *J. Phys. Chem.* **1990**, *94*, 8897−8909.
(17) Theodorou, D. N.; Suter, U. W. *Macromolecules* **1985**, *18*, 1206−1214.
(18) Lach, C.; Brizzolara, D.; Frey, H. *Macromol. Theory Simul.* **1997**, *6*, 371−380.
(19) Zhang, H.; Grim, P. C. M.; Foubert, P.; Vosch, T.; Vanoppen, P.; Wiesler, U.-M.; Berresheim, A. J.; Muellen, K.; De Schryver, F. C. *Langmuir* **2000**, *16*, 9009−9014.
(20) Scherrenberg, R.; Coussens, B.; van Vliet, P.; Edouard, G.; Brackman, J.; de Brabander, E. *Macromolecules* **1998**, *31*, 456−461.
(21) Boris, D.; Rubinstein, M. *Macromolecules* **1996**, *29*, 7251−7260.
(22) Lue, L. *Macromolecules* **2000**, *33*, 2266−2272.
(23) Gorman, C. B.; Smith, J. C. *Polymer* **2000**, *41*, 675−683.
(24) Mansfield, M. L. *Polymer* **1994**, *35*, 1827−1830.
(25) Chen, Z. Y.; Cui, S.-M. *Macromolecules* **1996**, *29*, 7943−7952.
(26) Wiener, H. *J. Am. Chem. Soc.* **1947**, *69*, 17−20.
(27) La Ferla, R. *J. Chem. Phys.* **1997**, *106*, 688−700.
(28) Diudea, M. V.; Pârv, B. *J. Chem. Inf. Comput. Sci.* **1995**, *35*, 1015−1018.

MA010953X